



# Study on long-wave infrared ZnGeP<sub>2</sub> subsequent optical parametric amplifiers with different types of phase matching of ZnGeP<sub>2</sub> crystals

Gaoyou Liu<sup>1</sup> · Yi Chen<sup>1</sup> · Baoquan Yao<sup>1</sup> · Ke Yang<sup>1</sup> · Chuanpeng Qian<sup>1</sup> · Tongyu Dai<sup>1</sup> · Xiaoming Duan<sup>1</sup>

Received: 15 August 2019 / Accepted: 10 November 2019 / Published online: 19 November 2019  
© Springer-Verlag GmbH Germany, part of Springer Nature 2019

## Abstract

Pumped by a 100 W Q-switched Ho:YAG laser at 2090.7 nm with pulse repetition frequency of 10 kHz, four types of high-power long-wave infrared ZnGeP<sub>2</sub> (ZGP) subsequent optical parametric amplifier (OPA) based on optical parametric oscillator (OPO) with different types of phase matching (PM) of ZGP crystals were demonstrated. For the results of 8.2 μm output characteristics at the full incident pump power, Type-II PM ZGP OPO with Type-II PM ZGP OPA had the best  $M^2$  of 1.8 and lowest average output power of 9.2 W with the narrowest linewidth of 77 nm, while Type-I PM ZGP OPO with Type-I PM ZGP OPA had the worst  $M^2$  of 2.2 and the widest linewidth of 122 nm, and Type-II PM ZGP OPO with Type-I PM ZGP OPA had the highest average output power of 12.6 W, corresponding to overall optical conversion efficiency of 12.6% from Ho to long-wave infrared laser system.

## 1 Introduction

High-power long-wave infrared laser sources are widely used in lidar, environmental monitoring and national defense. Compared with quantum cascade and II–VI group compound (ZnS/ZnSe/CdSe/CdTe) doped with transition metal ion (Tm<sup>2+</sup>/Cr<sup>2+</sup>/Fe<sup>2+</sup>/Co<sup>2+</sup>) as gain medium, the master-oscillator/power-amplifier (MOPA), that is to say optical parametric oscillator (OPO) and optical parametric amplifier (OPA) are better and efficient ways to obtain a high-power and tunable wide long-wave infrared (8–12 μm) spectral range with the nonlinear frequency conversion technology [1–3]. Zinc germanium phosphide (ZGP) has the combination of advantages of good thermal conductivity, high optical nonlinearity, high damage threshold and an optical transparency range of 2–12 μm [4–6] in comparison to AgGaS<sub>2</sub>, AgGaSe<sub>2</sub> and CdSe, so ZGP OPO and OPA are the effective methods to obtain long-wave infrared laser.

A ZGP OPO pumped at 2.9 μm with maximum pulse energy of 1 mJ at 8.1 μm was reported in 2000 by Vodopyanov et al. [7]. 0.95 W at 8 μm with beam quality factor  $M^2$  of 2.7 was obtained from ZGP OPO in 2007 by Lippert et al. [8]. Over 8 mJ at 8 μm by a ZGP OPA with  $M^2$  of 3.6 was

obtained in 2008 by Haakestad et al. [9]. They improved the average output power to 2.6 W at 8 μm by a three-mirror V-shaped ring resonator in 2011 [10].

For 8 μm, the idler beam from OPO can serve as the seed light of OPA and the signal beam from OPO can serve as the pump laser of OPA instead of an additional pump laser, which was called subsequent OPA and firstly demonstrated by Bakklund et al. in 2016, but the conversion efficiency of the OPA was only about 12% [11]. In 2018, pumped by a 2097 nm Q-switched Ho:YAG laser with pulse repetition frequency (PRF) of 20 kHz, Qian et al. demonstrated a ZGP subsequent OPA and obtained the maximum average output power of 11.4 W at 8.3 μm with  $M^2$  factor of 2.9 whose optical conversion efficiency from Ho to long-wave infrared was about 9.8% [12].

However, the existing comparison between the different types of PM of ZGP crystals in ZGP OPO and ZGP subsequent OPA is not systemic and overall up to now. According to the simulation of SNLO (a software of nonlinear crystals calculation), Type-I PM ZGP has a higher nonlinear coefficient of 80.9 pm/V than Type-II PM ZGP of 74.2 pm/V. The idler (8.2 μm) of Type-II PM ZGP both in OPO and OPA has no walk-off effect and the acceptance angle of pump dispersion for idler (8.2 μm) in Type-I PM ZGP is about 20 times to 30 times bigger than Type-II PM ZGP in OPO and OPA. So the difference between different types of PM of ZGP crystals in OPO and OPA will generate different output characteristics of idler (8.2 μm) in OPO and OPA.

✉ Baoquan Yao  
yaobq08@hit.edu.cn

<sup>1</sup> National Key Laboratory of Tunable Laser Technology, Harbin Institute of Technology, Harbin 150001, China

In this paper, we have demonstrated the ring ZGP OPO and ZGP subsequent OPA laser around 8.2  $\mu\text{m}$  pumped by a Q-switched Ho:YAG laser at 2090.7 nm with different types of PM of ZGP crystals: that is, Type-I PM ZGP OPO (I OPO), Type-II PM ZGP OPO (II OPO), Type-I PM ZGP OPO with Type-I PM ZGP OPA (I–I OPA), Type-I PM ZGP OPO with Type-II PM ZGP OPA (I–II OPA), Type-II PM ZGP OPO with Type-I PM ZGP OPA (II–I OPA) and Type-II PM ZGP OPO with Type-II PM ZGP OPA (II–II OPA). Generally speaking, 8  $\mu\text{m}$  ~ 12  $\mu\text{m}$  belongs to the range of long-wave infrared and the window of atmospheric transmission. Furthermore, the longer the wavelengths we produced, the lower was the output power we would get and the corresponding signal beam of OPO would be absorbed by water in the air more easily, leading to damage on the surface of the ZGP crystal in OPO. The spectrum of the idler beam was broadband, and the whole spectrum of the idler beam should be ensured larger than 8  $\mu\text{m}$  as far as possible. In conclusion, taking into account all the above factors, the peak wavelength of the idler beam at 8.2  $\mu\text{m}$  was chose. The aim of this paper is to study the output features and difference of different types of PM of ZGP subsequent OPA and the experimental results were measured in detail and compared. The work and results of this paper can provide reference for choosing different types of PM of ZGP crystals used in long-wave infrared.

## 2 Experimental setup

The schematic diagram of long-wave infrared ZGP MOPA experimental setup is shown in Fig. 1. The pump source was a s-polarized acousto-optical Q-switched Ho:YAG laser, whose maximum average output power was 100 W and PRF of 10 kHz. The Ho laser was forced to emit at a single wavelength of 2090.7 nm with a 0.05-mm-thickness YAG etalon inserted into the Ho:YAG resonator. The beam quality factors  $M^2$  of the Ho:YAG laser were 1.08 ( $x$  direction) and 1.10

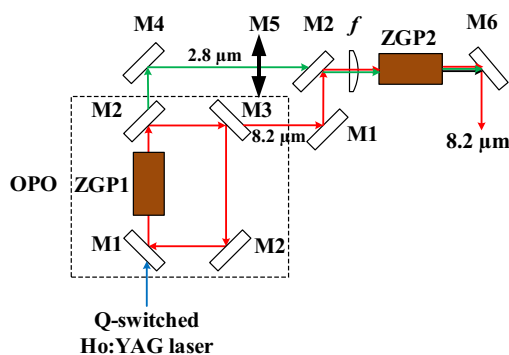


Fig. 1 Schematic diagram of the experimental setup

( $y$  direction) with pulse width of 23.5 ns at the maximum average output power. The high efficiency and brightness Ho:YAG laser was a MOPA system and dual-end-pumped by Tm:YLF lasers, which had a near diffraction limitation beam at the maximum output power. The Ho laser passed through a half-wave plate and a thin-film polarizer, and then got into the ZGP OPO, so we could change the injected pump power without altering the pump beam quality and the pulse width.

In this work, the first part was a long-wave infrared ZGP1 OPO with a rectangle configuration which consisted of four 45° flat mirrors. The  $1/e^2$  beam diameter of the Ho:YAG laser at the entrance surface of ZGP1 was about 1.6 mm. M1s was highly reflective (HR) at around 8  $\mu\text{m}$  for the s-polarized component and highly transparent (HT) at 2.1  $\mu\text{m}$  ( $T \sim 98.9\%$ ) for the p-polarized component. M2s was HR at around 8  $\mu\text{m}$  for the s-polarized component and HT at 2.8  $\mu\text{m}$  for the p-polarized component. The output coupler (M3) had a transmission of about 25% (no more output couplers with various transmissions in laboratory) at around 8  $\mu\text{m}$  for the s-polarized component and HT at 2.1  $\mu\text{m}$  for the p-polarized component. The ring ZGP1 OPO was then singly resonant and single-pass pumped. The physical cavity length of the ZGP1 OPO was about 170 mm. M4 was HR at around 2.8  $\mu\text{m}$  for the s-polarized component and HT at 2.1  $\mu\text{m}$  for the p-polarized component. Because the transmissivity of M4 and the second M1 at 2.1  $\mu\text{m}$  reached about 99%, the residual 2.1  $\mu\text{m}$  pump power after the OPO could be filtered before the OPA part, avoiding the parasitic conversion. A 2.8  $\mu\text{m}$   $1/2\lambda$  plate (M5) was inserted before the beam-combination mirror to change the polarized component of OPO signal (2.8  $\mu\text{m}$ ), which could satisfy the PM of I–I OPA and II–II OPA.

The signal (2.8  $\mu\text{m}$ ) and the idler (8.2  $\mu\text{m}$ ) of ZGP1 OPO were overlapped together and focused onto the ZGP2 by a plano-convex ZnSe lens with focal length 50 mm. The  $1/e^2$  beam diameter of the signal and idler of OPO at the entrance surface of ZGP2 was about 0.8–1.0 mm and 0.8–1.2 mm, respectively [12]. Then the idler beam from OPO served as the seed light of OPA, and the signal beam from OPO served as the pump laser of OPA to generate high-power long-wave infrared (8.2  $\mu\text{m}$ ) laser radiation by the subsequent OPA. M6 was HT for the 2.8  $\mu\text{m}$  ( $T \sim 98.8\%$ ) and 4.3  $\mu\text{m}$  ( $T \sim 97.5\%$ ) and HR for the 8.2  $\mu\text{m}$ . Two M6 were used to fully separate and measure 8.2  $\mu\text{m}$  from 2.8  $\mu\text{m}$  and 4.25  $\mu\text{m}$  of the OPA part. All the ZGP crystals (School of Chemical Engineering & Technology, HIT) were cut from the same ingots of ZGP and wrapped in indium foil and installed into copper blocks which were water cooled, so the temperature of ZGP crystals was controlled at approximately 16 °C by the water-cooling machine, and both the end surfaces of the ZGP crystals were coated with HT of 2.1  $\mu\text{m}$ , 2.8  $\mu\text{m}$ , 4.3  $\mu\text{m}$  and 8.2  $\mu\text{m}$ . The absorption coefficient of the ZGP crystals at 2.1  $\mu\text{m}$  was

less than that at  $0.03\text{ cm}^{-1}$ . To make full use of the  $2.1\text{ }\mu\text{m}$  pump and as a consequence of the above mirror coating, the Ho pump beam was changed from s-polarized component to p-polarized component by a  $2.1\text{ }\mu\text{m}$   $1/2\lambda$  plate for I OPO (not shown in the Fig. 1). Before putting the ZGP crystal in the OPA part, the  $2.8\text{ }\mu\text{m}$  signal beam was made collimating and to spatially overlap with He–Ne light after the third M2 and lens  $f$  at about 10 W by adjusting M4, and then the second M1 and third M2 were adjusted to make the  $8.2\text{ }\mu\text{m}$  idler beam spatially overlap with He–Ne light after the third M2 and lens  $f$  at full power. So, the  $2.8\text{ }\mu\text{m}$  signal beam and  $8.2\text{ }\mu\text{m}$  idler beam spatially overlapped before being injected into the ZGP crystal of OPA. The second M1 was slightly adjusted to make the  $8.2\text{ }\mu\text{m}$  output power of OPA biggest at full pump power.

### 3 Experimental results and discussions

#### 3.1 ZGP subsequent OPA system based on I OPO

The ZGP1 crystal had an aperture of  $6\text{ mm}\times 6\text{ mm}$  and  $25\text{ mm}$  long, cut at an angle of  $\theta=50.8^\circ$  with respect to Type-I PM. Based on the above ring ZGP1 OPO cavity, the threshold pump power was about 14 W and the maximum average output power of the ZGP1 OPO was about 7.2 W at  $8.2\text{ }\mu\text{m}$  and 35.5 W at  $2.8\text{ }\mu\text{m}$ , corresponding to the slope efficiency of about 8.8% and 43.9% with the pump of 100 W at  $2.1\text{ }\mu\text{m}$ . Two ZGP crystals in the OPO were broken on the surface with the pump power of 110 W, so the maximum pump power was limited at 100 W to avoid more damage.

At the maximum output level, the pulse width of the idler ( $8.2\text{ }\mu\text{m}$ ) of 20.2 ns was achieved in the ZGP1 OPO. The beam quality factor  $M^2$  of  $8.2\text{ }\mu\text{m}$  at the maximum output power was measured and fitted by using the 90/10 knife-edge method with a ZnSe lens. The  $M^2$  factor was calculated to be 1.9 by fitting the Gaussian beam standard expression. The

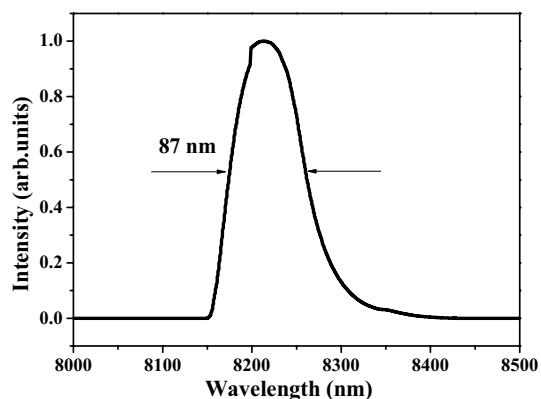


Fig. 2 Output spectrum of I OPO at  $8.2\text{ }\mu\text{m}$

output spectrum of  $8.2\text{ }\mu\text{m}$  of ZGP1 OPO was measured by a 150 mm WDG30-Z monochromator, HgCdTe detector and Tektronix oscilloscope ( $300\text{ MHz}$   $2.5\text{ GS/s}$ ). As shown in Fig. 2, the central wavelength of the idler light was around  $8.2\text{ }\mu\text{m}$ , corresponding to a broad output spectrum envelop with an FWHM of 87 nm.

The first ZGP2 crystal used in the ZGP subsequent OPA system was cut for Type-I PM ( $\theta=48.4^\circ$  and  $\varphi=0^\circ$ ) with dimensions of  $6\times 6\text{ mm}^2$  (in cross section) $\times 25\text{ mm}$  (in length). Then the ZGP2 crystal was replaced by another ZGP which was cut for Type-II PM ( $\theta=68.4^\circ$  and  $\varphi=45^\circ$ ) with dimensions of  $6\times 6\text{ mm}^2$  (in cross section) $\times 25\text{ mm}$  (in length). With the incident Ho pump power of 100 W, the  $8.2\text{ }\mu\text{m}$  output characteristics of ZGP subsequent OPA with the above two types of PM of ZGP crystals are shown in Table 1. Figures 3, 4 and 5 show the average output powers,  $M^2$  factors and output spectrums of I–I OPA and I–II OPA at  $8.2\text{ }\mu\text{m}$ . Figure 3 indicates that the idler ( $8.2\text{ }\mu\text{m}$ ) of I OPO was apparently amplified with the signal beam from OPO serving as the pump laser of ZGP2 OPA.

#### 3.2 ZGP subsequent OPA system based on II OPO

The ZGP1 crystal was cut for Type-II PM ( $\theta=64.6^\circ$  and  $\varphi=45^\circ$ ) with dimensions of  $6\times 6\text{ mm}^2$  (in cross section) $\times 25\text{ mm}$  (in length). When implementing the OPO with type-II ZGP and the subsequent OPA experiment, all the mirrors/output couplers were retained. By adjusting the

Table 1  $8.2\text{ }\mu\text{m}$  characteristics of ZGP OPA based on I OPO

Type of PM	Size of ZGP mm	Output power W	Pulse width ns	$M^2$	Linewidth (FWHM) nm
I	$6\times 6\times 25$	11.5	20.9	2.2	122
II	$6\times 6\times 25$	9.7	21.1	2.0	99

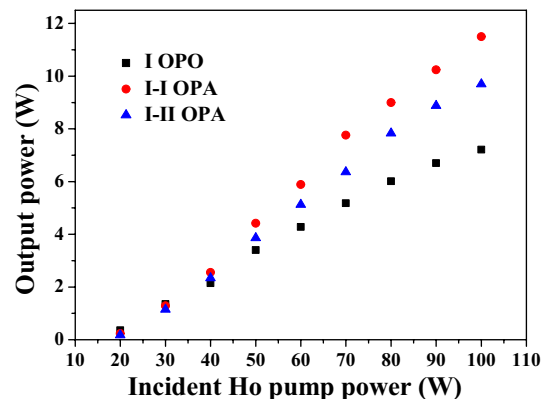


Fig. 3 Average output powers of I–I OPA and I–II OPA at  $8.2\text{ }\mu\text{m}$

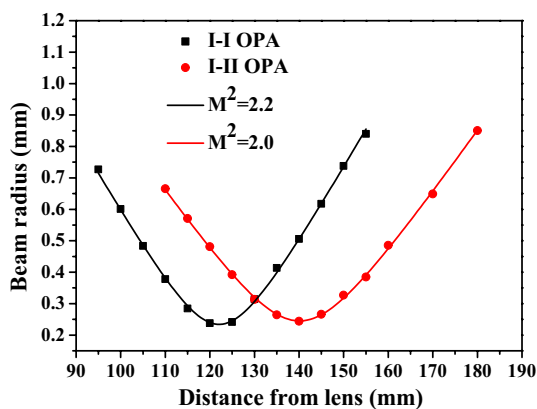


Fig. 4 Beam propagation and  $M^2$  factors of I-I OPA and I-II OPA at  $8.2 \mu\text{m}$

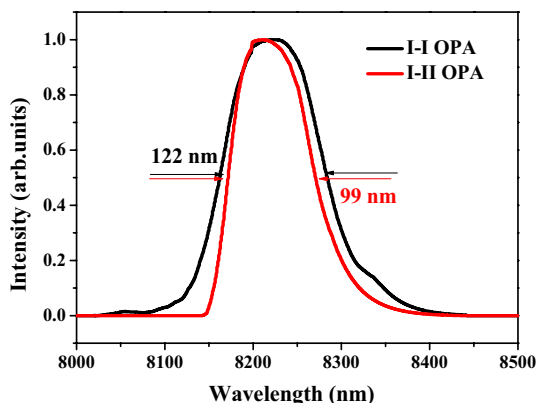


Fig. 5 Output spectra of I-I OPA and I-II OPA at  $8.2 \mu\text{m}$

$2.09 \mu\text{m}$  half-wave plate mentioned above could keep the incident pump p-polarized for I OPO and s-polarized for II OPO to ensure the vibration light ( $8.2 \mu\text{m}$  idler beam) in both OPO keeps s-polarized. Then the inserted  $2.8 \mu\text{m}$  half-wave plate ( $M5$ ) could change the polarized component of OPO signal ( $2.8 \mu\text{m}$ ) to satisfy the phase matching of I-I OPA and II-II OPA. Furthermore, the reflectivity and transmissivity of glass filters ( $M2$  s,  $M4$ ,  $M6$ ) used in the experimental setup for p-polarized and s-polarized at corresponding wavelength showed no obvious discrepancy. With the same ring ZGP1 OPO cavity and the pump of  $100 \text{ W}$  at  $2.1 \mu\text{m}$ , the threshold pump power was about  $15.5 \text{ W}$  and the maximum average output power of the ZGP1 OPO was about  $7.3 \text{ W}$  at  $8.2 \mu\text{m}$  and  $36.0 \text{ W}$  at  $2.8 \mu\text{m}$ , corresponding to the slope efficiency of about  $8.8\%$  and  $42.9\%$ .

The pulse width and  $M^2$  of the idler ( $8.2 \mu\text{m}$ ) was  $20.9 \text{ ns}$  and  $1.6$  at the maximum output level in the ZGP1 OPO. As shown in Fig. 6, the central wavelength of the idler light was around  $8.2 \mu\text{m}$  and the FWHM of the output spectrum was approximately  $66 \text{ nm}$ .

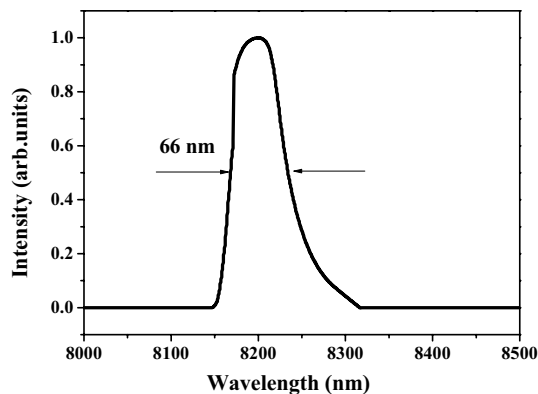


Fig. 6 Output spectrum of II OPO at  $8.2 \mu\text{m}$

Table 2  $8.2 \mu\text{m}$  characteristics of ZGP OPA based on II OPO

Type of PM	Size of ZGP mm	Output power W	Pulse width ns	$M^2$	Linewidth (FWHM) nm
I	$6 \times 6 \times 25$	12.6	21.5	2.1	89
II	$6 \times 6 \times 25$	9.2	21.4	1.8	77

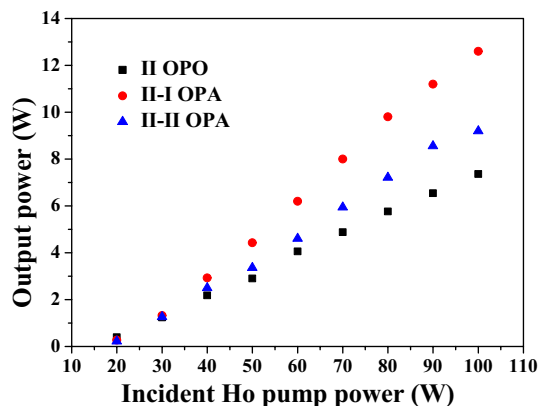
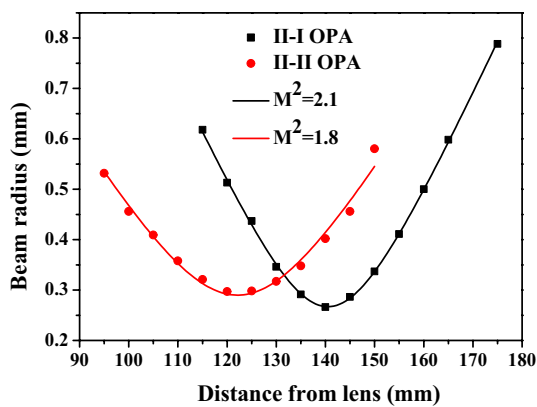


Fig. 7 Average output powers of II-I OPA and II-II OPA at  $8.2 \mu\text{m}$

With the incident Ho pump power of  $100 \text{ W}$ , the  $8.2 \mu\text{m}$  output characteristics of ZGP subsequent OPA with the two types of PM of ZGP2 crystals used above are shown in Table 2. The average output powers,  $M^2$  factors and output spectra of II-I OPA and II-II OPA at  $8.2 \mu\text{m}$  are shown in Figs. 7, 8 and 9

Table 3 shows a summarization of output power, pulse width,  $M^2$  and linewidth in ZGP OPO and OPA of different types of PM at  $8.2 \mu\text{m}$ . For ZGP OPO, based on the Sellmeier equations given in Ref [5] and the formula (1):



**Fig. 8** Beam propagation and M2 factors of II-I OPA and II-II OPA at 8.2 μm

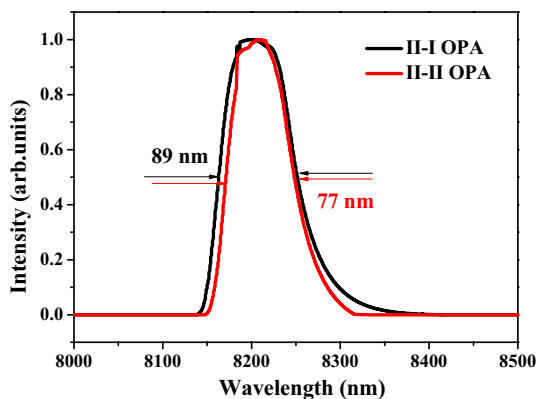


**Fig. 9** Output spectrums of II-I OPA and II-II OPA at 8.2 μm

$$\Delta\lambda = \frac{\lambda_i^2}{l} \left( n_i - n_s + \lambda_s \frac{\partial n_s}{\partial \lambda_s} - \lambda_i \frac{\partial n_i}{\partial \lambda_i} \right)^{-1}, \tag{1}$$

the theoretical gain bandwidth (TGB) (theoretical full and width) was estimated and is shown in Table 3, where  $\lambda_i$  is the idler wavelength,  $\lambda_s$  the signal wavelength,  $l$  the crystal length,  $n_i$  the refractive index of the idler and  $n_s$  the

refractive index of the signal. Probably owing to the difference between Sellmeier equations used in formula (1) and the actual experiment, and the shortage of consideration of gain of different wavelength when the wavelength broadened, the experimental full bandwidth was larger than that of the TGB.

Table 3 and the results showed that, for the part of ZGP OPO with the same pump power and same ring cavity, I OPO and II OPO had similar average output power, while II OPO had narrower linewidth and better  $M^2$ . From the ZGP crystal angular tuning curve [5] of long-wave infrared band for Type-I PM and Type-II PM, we know that compared with Type-II PM ZGP, Type-I PM ZGP had a bigger wavelength range of variation with the same PM angle change, which indicated that ZGP crystals of Type-I PM had a wider acceptance of linewidth to proceed with nonlinear frequency conversion in ZGP OPO or ZGP OPA. So the linewidth in I OPO was wider than in II OPO. The idler (8.2 μm) of II OPO had no walk-off effect while the idler of I OPO had, so the II OPO had better  $M^2$ .

As for the ZGP subsequent OPA, I-I OPA had the worst  $M^2$  and widest linewidth, II-I OPA had the highest average output power, while the II-II OPA had the best  $M^2$  and lowest average output power with the narrowest linewidth.

Because the idler (8.2 μm) of II OPO had no walk-off effect while the idler of I OPO had, the I-I OPA had the worst  $M^2$  and the II-II OPA had the best  $M^2$ .

Although calculated by SNLO, Type-I phase match was more efficient than Type-II, but II-I OPA got the highest average output power of 8.2 μm in the experiment. This result could be explained as follows: because the maximum average output powers of 2.8 μm and 8.2 μm in I OPO were almost the same with that in II OPO, the average power of seed light and pump light was approximately equal in the four types of ZGP subsequent OPA. But the linewidths of 2.8 μm and 8.2 μm in II OPO were narrower than that of I OPO, and the OPA with Type-I PM ZGP had a wider acceptance of linewidth, so that 2.8 μm and 8.2 μm in II OPO could proceed with optical parametric amplification in a wider range of output spectrums in II-I OPA. The average output powers of 2.8 μm and 8.2 μm for single wavelength

**Table 3** 8.2 μm characteristics of ZGP OPO and OPA of different types of PM

	Type of PM	Size of ZGP mm	Output power W	Pulse width ns	$M^2$	Linewidth(FWHM) nm	Full bandwidth nm	TGB nm
OPO	I	6×6×25	7.2	20.2	1.9	87	279	190
OPA	I-I	6×6×25	11.5	20.9	2.2	122		
OPA	I-II	6×6×25	9.7	21.1	2.0	99		
OPO	II	6×6×25	7.3	20.9	1.6	66	170	60
OPA	II-I	6×6×25	12.6	21.5	2.1	89		
OPA	II-II	6×6×25	9.2	21.4	1.8	77		

in II OPO were higher than I OPO because of its narrower linewidth, corresponding to the average power of seed light and pump light preceding optical parametric amplification in OPA were higher than I OPO. Owing to the above reasons, II–I OPA had the highest average output power of 8.2  $\mu\text{m}$ , and on the contrary II–II OPA had the lowest average output power of 8.2  $\mu\text{m}$ .

With regard to 8.2  $\mu\text{m}$  linewidth of OPA, because the Type-I PM ZGP had a bigger wavelength range of variation than Type-II with the same PM angle change, I–I OPA had the widest linewidth and II–II OPA had the narrowest linewidth.

## 4 Conclusion

In conclusion, we demonstrated high-power long-wave infrared ZGP subsequent OPA system with different types of PM ZGP crystals pumped by a 100 W Q-switched Ho:YAG laser at 2090.7 nm with PRF of 10 kHz and discussed the results of 8.2  $\mu\text{m}$  output characteristics. With regard to 8.2  $\mu\text{m}$  in ZGP OPO, I OPO and II OPO had similar average output power, while II OPO had a narrower linewidth of 66 nm and better  $M^2$  of 1.6. In regard to the results of 8.2  $\mu\text{m}$  in the four types of ZGP subsequent OPA, I–I OPA had the worst  $M^2$  of 2.2 and the widest linewidth of 122 nm, and II–I OPA had the highest average output power of 12.6 W, corresponding to overall optical conversion efficiency of 12.6% from Ho to long-wave infrared laser system, while II–II OPA had the best  $M^2$  of 1.8 and the lowest average output power of 9.2 W with the narrowest linewidth of 77 nm. This work can provide reference for choosing different types of PM of ZGP crystals used in long-wave infrared.

**Acknowledgements** This work was supported by the National Natural Science Foundation of China (NSFC) (61378029, 51572053 and

61775053), Science Fund for Outstanding Youths of Heilongjiang Province (JQ201310), Fundamental Research funds for the Central Universities (HIT.NSRIF.2014044, and 2015042) and Fundamental Research funds for the Provincial Universities (WL17B14).

## References

1. Y. Bao-Quan, L. Gang, Z. Guo-Li, M. Pei-Bei, J. You-Lun, W. Yue-Zhu, *Chin. Phys. B* **21**(3), 034213 (2012)
2. V. Petrov, *Prog. Quant. Electron* **42**, 1–106 (2015)
3. M.E. Webber, M. Pushkarsky, C.K.N. Patel, *J. Appl. Phys.* **97**, 113101 (2005)
4. K. Scholle, S. Lamrini, P. Koopmann, P. Fuhrberg, in *Frontiers in Guided Wave Optics and Optoelectronics* (Intech Open, 2010)
5. D.E. Zelmon, E.A. Hanning, P.G. Schunemann, *JOSA B* **18**, 1307–1310 (2001)
6. K. L. Vodopyanov, V. G. Voevodin, *Opt. Commun*, **117** (1995)
7. K.L. Vodopyanov, F. Ganikhanov, J.P. Maffetone, I. Zwieback, W. Ruderman, *Opt. Lett* **25**, 841–843 (2000)
8. E. Lippert, G. Rustad, K. Stenersen, *Technologies for Optical Countermeasures IV. International Society for Optics and Photonics* **6738**, 67380D (2007)
9. M.W. Haakestad, G. Arisholm, E. Lippert, S. Nicolas, G. Rustad, K. Stenersen, *Opt. Express* **16**, 14263–14273 (2008)
10. E. Lippert, *Technologies for Optical Countermeasures VIII. International Society for Optics and Photonics* **8187**, 81870F (2011)
11. A. Bakklund, H. Fonnum, E. Lippert, M. W. Haakestad, in *CLEO: Science and Innovations* (Optical Society of America, STu1Q. 8, 2016)
12. C.P. Qian, X.M. Duan, B.Q. Yao, Y.J. Shen, Y. Zhang, B.R. Zhao, J.H. Yuan, T.Y. Dai, Y.L. Ju, Y.Z. Wang, *Opt. Express* **26**, 30195–30201 (2018)

**Publisher's Note** Springer Nature remains neutral with regard to jurisdictional claims in published maps and institutional affiliations.